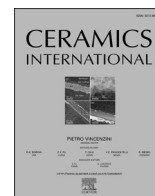




Contents lists available at ScienceDirect

Ceramics International

journal homepage: www.elsevier.com/locate/ceramint

Bulk composite of silica and detonation nanodiamonds with partially removed sp^2 shells

M.A. Korotkova^{a,*}, V.S. Efimchenko^a, V.E. Antonov^a, O.I. Barkalov^a, I.G. Fomina^b,
T.N. Fursova^a, K.A. Gavrilicheva^a, S.V. Zaitsev^a, I.O. Gozhikova^c, A.Ya. Vul'^d,
S.A. Lermontov^c

^a Institute of Solid State Physics RAS, 142432, Chernogolovka, Moscow District, Russia

^b Kurnakov Institute of General and Inorganic Chemistry RAS, 119991, Moscow, Russia

^c Institute of Physiologically Active Compounds at Federal Research Center of Problems of Chemical Physics and Medicinal Chemistry RAS, 142432, Chernogolovka, Moscow District, Russia

^d Ioffe Institute, 194021, St. Petersburg, Russia

ARTICLE INFO

Keywords:

Pressing (A)

Composites (B)

Detonation nanodiamonds (–)

SiO₂ (D)

ABSTRACT

Diamonds with impurity-vacancy centers are an attractive material for microphotonics and can be used, for example, as single photon emitters. Detonation nanodiamonds (DNDs) with intrinsic single nitrogen-vacancy (NV) centers are cheap and suitable for mass production. This paper proposes a way to overcome the two main properties of the DNDs: the tendency to agglomeration and the presence of a thick shell of sp^2 -hybridized carbon around each detonation nanodiamond particle. It is shown that SiO₂ aerogel with uniformly distributed single diamond nanocrystals compressed to 7.5 GPa at 250 °C irreversibly transforms into a dense and chemically inert material. Subsequent treatment of this material in a hydrogen atmosphere at 7.5 GPa and 600 °C passivates dangling bonds in the silica matrix and eliminates its parasitic luminescence. The hydrogenation also largely removes the sp^2 shells from DNDs and converts their neutral NV⁰ centers into more useable negatively charged NV[–] centers. After each stage of preparing the dense DNDs/SiO₂ composite, the material was examined by X-ray diffraction and Infrared and Raman spectroscopy.

1. Introduction

In the development of new composite materials, considerable attention is paid to diamond nanoparticles synthesized by the detonation synthesis method and known as detonation nanodiamonds (DNDs) [1–3]. The interest in such materials is due to the unique properties of diamond, such as high thermal conductivity, chemical inertness and record mechanical characteristics, which can be used in composites. In the last two decades, particular attention has been attracted to the diamond nanoparticles with a high concentration of luminescent (or color) centers, which are negatively charged nitrogen vacancy (NV[–]) centers. Their unique energy structure ensures high sensitivity of photoluminescence in the visible spectral region to external influences, such as magnetic and electric fields, temperature and pressure [4].

The preferential development of research on NV centers compared to other color centers, such as SiV, is due to the high concentration of

impurity nitrogen atoms in diamond crystals. Indeed, in the traditional synthesis of diamonds from graphite at high pressures and temperatures (HPHT) in the presence of a metal catalyst, the concentration of nitrogen reaches 50–100 ppm. The high nitrogen concentration is due to the capture of nitrogen atoms by the diamond crystal growing from the molten metal catalyst. The source of nitrogen in HPHT is the air present in the pores of the high-pressure cell [5]. The generally accepted technology for creating NV centers is to generate vacancies by irradiation with protons or electrons and subsequent high-temperature annealing, which ensures the diffusion of vacancies [6,7].

During the detonation synthesis of diamonds, the formation of NV centers occurs according to a similar scheme: irradiation with protons or electrons followed by thermal annealing. The high concentration of nitrogen in DNDs is due to the presence of nitrogen in the explosives used [1,2]. Currently, two main technologies for obtaining diamond nanoparticles with NV centers are being developed in parallel: mechanical

* Corresponding author.

E-mail address: korotkova@issp.ac.ru (M.A. Korotkova).

<https://doi.org/10.1016/j.ceramint.2025.03.197>

Received 25 December 2024; Received in revised form 26 February 2025; Accepted 13 March 2025

Available online 14 March 2025

0272-8842/© 2025 Elsevier Ltd and Techna Group S.r.l. All rights are reserved, including those for text and data mining, AI training, and similar technologies.

crushing and fractionation of bulk diamond single crystals synthesized by the HPHT method, or disaggregation and fractionation of DNDs [8].

Comparing these two technologies, it should be noted that the production of nanoparticles with a diameter of ≤ 10 nm from HPHT diamonds is a multi-stage and complex process, which limits their use, for example, as biomarkers [9] or single-photon emitters [10]. At the same time, DNDs, synthesized by the most common industrial method from a mixture of 2,4,6-trinitrotoluene (TNT) and cyclotrimethylenetrinitramine (RDX) [11], have a crystal size of 4–5 nm [1,2,8]. However, these particles form strong aggregates with a hierarchical structure [12,13].

Present-day methods of mechanical disaggregation make it possible to obtain powders and stable hydrosols of DNDs nanoparticles with the size of 4–5 nm [12–14]. However, the disaggregation changes the surface structure of the nanoparticles, and at a depth of 2–3 atomic layers, the hybridization of the electron orbitals of carbon is transformed from sp^3 (diamond) to sp^2 (graphite) leading to the formation of “onion-like carbon”. This causes strong optical absorption in the visible spectrum, so the particles still remain unsuitable for use as biomarkers [15,16] or single photon emitters for quantum applications [10]. Obviously, the formation of an optically transparent nanoparticle of detonation diamond requires either the removal of the “ sp^2 shell”, or a change in the type of hybridization of carbon atoms on its surface from sp^2 to sp^3 .

Among the various applications of fluorescent diamond nanoparticles discussed in Ref. [17], the possibility of their use in medicine in combination with silica materials is considered, for example, in drug delivery systems [18]. In addition, Ref. [19] pointed out the possibility of using a durable DNDs/SiO₂ composite coating for low temperature sensors that are resistant to external influences.

The goal of our work was to study the possibility of embedding individual detonation nanodiamonds with luminescent NV⁻ centers, active at room temperature, into a massive silicon matrix that is transparent in the visible range and protects the nanodiamonds from negative external factors.

In our recent work [20], we developed a method based on the sol-gel SL protocol to prepare DNDs/SiO₂ aerogels, in which individual 4–5 nm surface carboxylated DNDs particles are uniformly distributed within silica aerogel cells. The SiO₂ aerogel is hydrophilic [21], brittle [22] and exhibits strong parasitic luminescence [23], making it unsuitable for many applications. However, since the aerogel already contains well separated and immobilized individual nanodiamonds, it can be used as a starting material to produce a bulk composite by irreversibly compacting the material at high pressures and temperatures.

The composite is expected to no longer be brittle compared to the aerogel. Nevertheless, the DNDs particles embedded in the compressed silica matrix will remain covered with sp^2 shells. The shells not only prevent light from passing into and out of the particles but also act as electron traps and hamper the conversion of neutral NV⁰ centers into negatively charged NV⁻ centers with optical and spin properties desirable for applications [24,25].

The conversion of sp^2 into sp^3 is possible as a result of thermal treatment of the material in hydrogen, as follows from the technology of CVD synthesis of diamond films. In the case of nanoparticles of detonation diamond, the effectiveness of such treatment was experimentally confirmed in Ref. [26]. On the other hand, the surface carboxyl groups present on the sp^2 shells are necessary for stabilizing the initial aqueous suspension of disaggregated nanodiamonds and subsequent synthesis of the aerogel [20,27]. Therefore, the sp^2 shells can be passivated or removed by hydrogen no earlier than the DNDs/SiO₂ aerogel is prepared. However, in this case, the nanodiamond will be surrounded by silica and the rate of reaction between the H₂ and sp^2 shell will be controlled by the amount of molecular hydrogen dissolved in the SiO₂. The solubility of hydrogen in SiO₂ is known to significantly increase with increasing pressure. For example, at a pressure of 7.5 GPa, the solubility of molecular hydrogen in silica glass reaches a molar ratio of $X = 0.7$ [28], while at pressures of several tens of atmospheres it does not exceed thousandths of this ratio [29]. Consequently, the hydrogenation

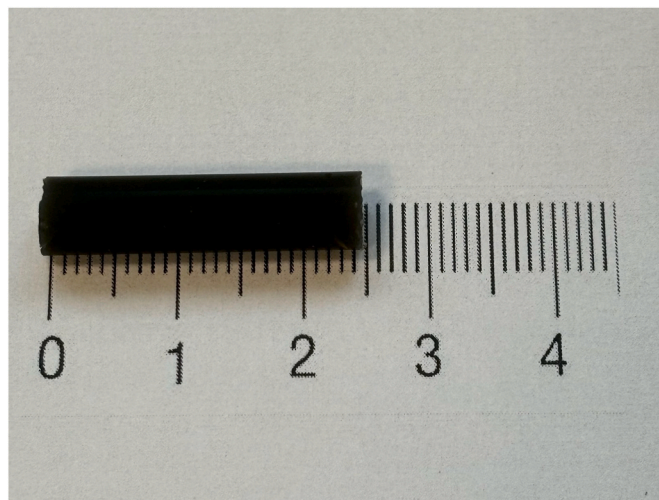


Fig. 1. A photo of a rod of the SiO₂ aerogel with 6 wt% DNDs annealed in air at 400 °C for 4 h.

of the sp^2 shells of DNDs is best carried out on a DNDs/SiO₂ composite already compacted at a pressure of 7.5 GPa. In addition, the pressure of 7.5 GPa is within the thermodynamic stability range of diamond, which prevents a possible sp^3 to sp^2 transition in nanodiamonds [30]. The temperature of 600 °C that we chose for the hydrogenation at a pressure of 7.5 GPa is low enough to avoid the reaction of carbon and hydrogen with the SiO₂ matrix and to exclude the formation of compounds such as SiC [31], SiH₄ and H₂O [32]. The interaction of high-pressure hydrogen with sp^2 carbon of the DNDs embedded in a SiO₂ matrix has never been studied before.

Based on previous high-pressure studies of the graphite-hydrogen system [33], we planned to make use of one or both of the two possible reactions, each of which should lead to the destruction of the nanodiamonds shell. First, at a hydrogen pressure of 7.4 GPa and temperatures up to about 700 °C, bulk graphite forms sp^3 multilayer graphane, a dielectric with a large electron band gap and composition CH. Second, at the same pressure and temperatures above approximately 750 °C, multilayer graphane and hydrogen form methane and/or other light hydrocarbons.

In this work, the luminescence of the SiO₂ matrix and the NV⁰ centers in nanodiamonds was suppressed, and the shells themselves were largely removed by hydrogenating the pre-compressed DNDs/SiO₂ pellets at a hydrogen pressure of 7.5 GPa and a temperature of 600 °C. The hydrogen that diffused through the SiO₂ matrix apparently passivated the dangling bonds and other defects remaining on the previous surface layers of the aerogel and on the sp^2 shells of the nanodiamonds. Most importantly, the removal of the sp^2 shell of the DNDs transferred most of the NV centers in the diamond cores to the negatively charged NV⁻ state, so that the luminescence of these centers became much more intense than the remaining parasitic luminescence of the SiO₂ matrix.

2. Experimental details

The initial amorphous SiO₂ aerogel containing 6 wt% DNDs uniformly distributed over its volume (molecular ratio C/SiO₂ \approx 0.29) was prepared using commercially available analytical-grade reagents and solvents. Hydrosol of surface carboxylated DNDs (1 wt% in deionized water, ash content less than 0.1 %) was prepared according to Ref. [34].

Its 6 wt% suspension was prepared by a gentle evaporation of 40 g of the initial 1 wt% hydrosol to 7.2 g with a rotary evaporator. To convert the suspension into aerogel, tetramethyl orthosilicate (Si(OMe)₄ or TMOS) and DMSO from Acros Organics; 25 wt% NH₄OH solution from Sigma Tech, and isopropanol (i-PrOH) from Sigma Aldrich were used as received. The aerogel with 6 wt% DNDs was prepared from 1.11 g of

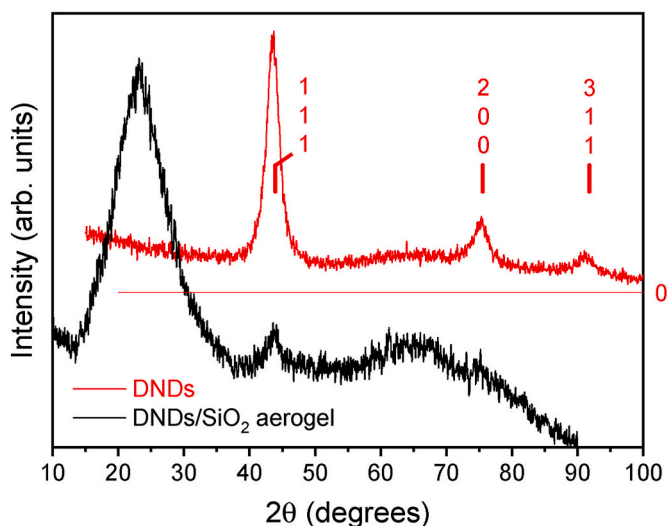


Fig. 2. X-ray diffraction patterns of the initial DNDs (red curve) and SiO₂ aerogel containing 8.5 wt% DNDs (black curve). Room temperature, Cu K α radiation. (For interpretation of the references to color in this figure legend, the reader is referred to the Web version of this article.)

TMOS (providing 0.44 g of SiO₂ after hydrolysis), 1.67 mL of DMSO, and 0.52 mL of 6 wt% DNDs hydrosol in deionized water (28 mg of dry DNDs) by a recently described NH₄OH catalyzed sol-gel protocol [20]. The 8.5 wt% DNDs suspension for aerogel with 8.5 wt% DNDs was prepared by evaporation of 48 g of the initial 1 wt% hydrosol to 6.2 g. The DNDs/SiO₂ gel thus formed was washed by 10 mL of i-PrOH five times (each wash lasted 24 h) and placed into an autoclave for supercritical drying. The drying was carried out in a CO₂ atmosphere at 50 °C and 15 MPa using an installation composed of a high-pressure CO₂ pump (SSI Supercritical 24, USA), a 50 mL steel reactor, and a back pressure regulator (Waters BPR, USA). The resulting material in the form of a rod 4 mm in diameter and 25 mm long (see Fig. 1) was placed in an aluminum crucible and annealed in air at 400 °C for 4 h in order to reduce the amount of adsorbed water and hydroxyl groups [35,36]. When not in use, the annealed rod was stored in an Ar glove box. The average size of nanodiamonds embedded in its amorphous SiO₂ matrix was ~5 nm, including the outer sp² shell 1–1.5 nm thick [20].

High-pressure treatments were carried out in Toroid-type quasi-hydrostatic chambers [37] at a pressure of 7.5 GPa, i.e., in the pressure range where diamond is more thermodynamically stable than graphite [30]. To obtain a compacted material, the initial aerogel was placed into a Teflon cell between two steel disks, isolated from the aerogel with palladium foil, and exposed to 7.5 GPa and 250 °C for 17 h. The resulting dense and opaque pellet of the DNDs/SiO₂ composite with a diameter of 5 mm and thickness of 0.7 mm was further hydrogenated at an H₂ pressure of 7.5 GPa and a temperature of 600 °C for 1 h. The reaction cell was made of silver. Hydrogen inside the cell was produced by thermal decomposition of aminoborane NH₃BH₃, which was placed in the cell together with the pellet of the composite and used as an internal hydrogen source. The pellet was wrapped in Pd foil to protect the composite from reaction with by-products formed during the intermediate stages of thermal decomposition of NH₃BH₃. The amount of gaseous H₂ released from NH₃BH₃ was 6 times greater than the amount of hydrogen absorbed by the sample and Pd foil. The method of hydrogenation is described in more detail elsewhere [33,38].

Before releasing the pressure, the compacted and hydrogenated samples of the DNDs/SiO₂ composite were cooled to room temperature together with the high-pressure chamber. When not in use, both samples were further stored in an argon glove box.

The initial, as well as the compacted and hydrogenated samples of DNDs embedded in the SiO₂ matrix were examined by X-ray diffraction

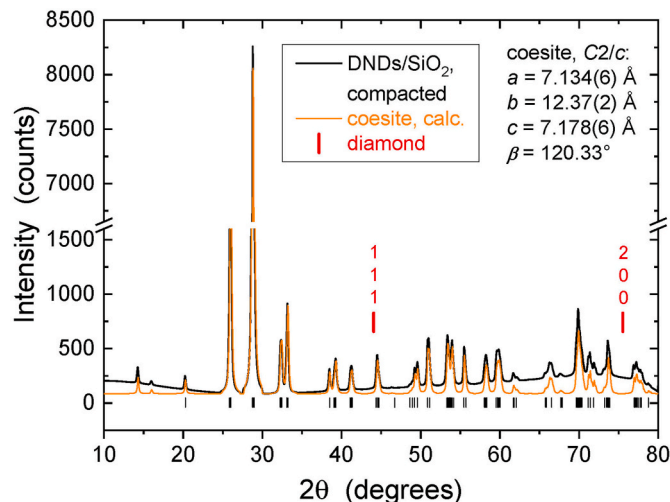


Fig. 3. X-ray diffraction pattern of SiO₂ aerogel containing 6 wt% DNDs and compacted at 7.5 GPa and 250 °C (black curve) and its profile fit based on the monoclinic C2/c crystal structure of coesite (orange curve). The vertical bars show the expected positions of diffraction peaks of coesite (black) and diamond (red). Room temperature, Cu K α radiation. (For interpretation of the references to color in this figure legend, the reader is referred to the Web version of this article.)

and infrared (IR) and Raman spectroscopy under ambient conditions. The X-ray diffraction studies were carried out with a Siemens D500 diffractometer using Cu K α radiation selected with a diffracted beam monochromator; the obtained diffraction patterns were analyzed using POWDERCELL2.4 software. The IR spectra were measured in the spectral range 400–4000 cm⁻¹ on a Vertex 80v FTIR spectrometer with a spectral resolution of 2 cm⁻¹. Samples for the IR measurements were ground in an agate mortar and then applied as a thin layer onto a polished crystal substrate made of KBr. The Raman spectra were studied on an HRS-500 spectrometer using a laser with a wavelength of ~532 nm.

To determine the hydrogen content of the hydrogenated composite, its small portion of several milligrams was analyzed by hot extraction of the hydrogen into a pre-evacuated calibrated volume in the regime of heating the sample to 655 °C at a rate of 20 °C/min (see Ref. [33] for details).

3. Results

3.1. X-ray diffraction

The red curve in Fig. 2 shows an X-ray diffraction pattern of DNDs obtained from the initial DNDs hydrosol by complete evaporation of water. The half-width at half-maximum of the diffraction peaks corresponds to nanodiamonds with a size of ~5 nm. To make the strongest 111 diffraction peak of nanodiamonds embedded in the SiO₂ aerogel clearly visible, the black curve shows the diffraction pattern of a sample containing 8.5 wt% DNDs in SiO₂ aerogel (molecular ratio C/SiO₂ ≈ 0.41).

Compression to 7.5 GPa at a temperature of 250 °C transformed the porous, brownish and translucent SiO₂ aerogel with 6 wt% DNDs into a dense, dark and opaque material. As seen from its X-ray diffraction pattern shown in Fig. 3, the amorphous matrix of this material crystallized into coesite, a high-pressure monoclinic phase of SiO₂ (space group C2/c, No. 15 [39]). No diffraction peaks from the nanodiamonds were observed, since i) the peaks were broadened (see Fig. 2) and ii) the X-ray scattering length of the carbon atoms was short compared to the silicon and oxygen atoms. The coesite matrix had a complex texture because it crystallized under non-uniform stress between two steel disks. The fitted coesite profile (orange curve) is shown without the calculated

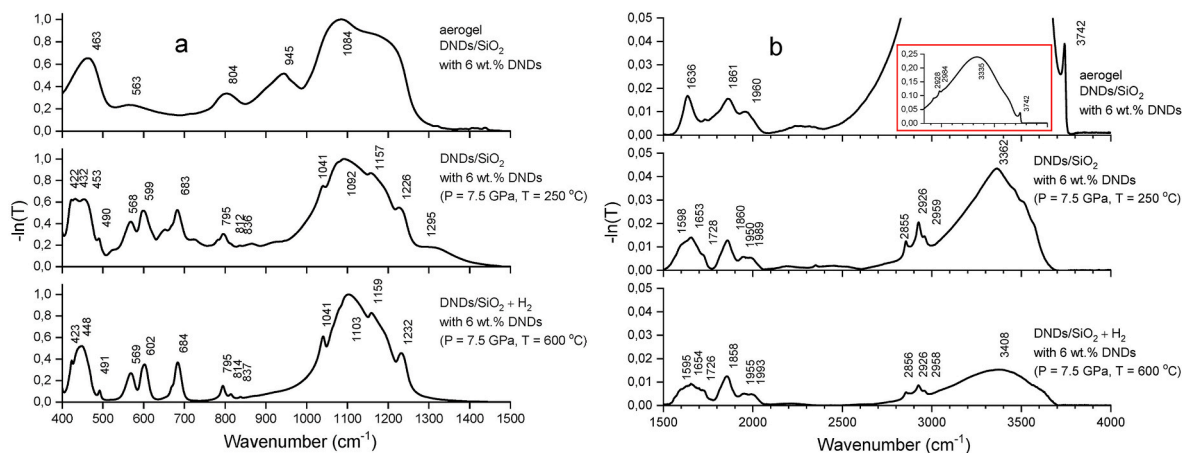


Fig. 4. Fig. 4a and b shows, respectively, the low-energy ($400\text{--}1500\text{ cm}^{-1}$) and high-energy ($1500\text{--}4000\text{ cm}^{-1}$) parts of the infrared transmission spectra of DNDs/SiO₂ samples containing 6 wt% DNDs. These are the samples of the initial aerogel (upper panels), the composite compacted at 7.5 GPa and 250 °C (middle panels), and this composite hydrogenated at 7.5 GPa and 600 °C (lower panels). The integral intensity of each peak is normalized to the intensity of the coesite peak at 1086–1103 cm⁻¹. In Fig. 4b, upper panel, the truncated top of the most intense peak is shown in the inserted smaller panel.

background to better visualize the intense broad halo extending from 20 ~50° to ~80° with a maximum at 70–75°. The halo might indicate the presence of some other amorphous or fine-crystalline phases.

The X-ray diffraction pattern of the hydrogenated DNDs/SiO₂ composite looked almost identical and also contained only coesite diffraction peaks.

3.2. Infrared spectroscopy

Fig. 4a and b shows IR spectra of the initial SiO₂ aerogel with nanodiamonds (upper panels), the same aerogel compacted under high pressure (middle panels) and then hydrogenated under high H₂ pressure (lower panels). For brevity, the sample compressed to 7.5 GPa at 250 °C will further be referred to as a compacted composite, and the sample hydrogenated at 7.5 GPa at 600 °C as a hydrogenated composite.

In the IR spectrum of the initial aerogel, remarkable absorption bands are observed around 463, 804, and 1084 cm⁻¹. These bands are characteristic of amorphous silicon dioxide and can be assigned to the O–Si–O bending vibration and to the Si–O–Si symmetric and antisymmetric stretching vibration, respectively [40]. The spectrum of the initial aerogel shows peaks at 563 and 945 cm⁻¹ (Fig. 4a), which can be attributed to the Si–O stretching vibrations of defects in the SiO₂ network and to the Si–OH stretching vibration of surface silanol groups, respectively [41]. Weak bands at 1636, 1861, and 1960 cm⁻¹ (Fig. 4b) can be attributed to the H–O–H bending mode of water molecule and combinations of the silicon-oxygen fundamentals, respectively [42]. In addition, one can see a broad band centered at 3338 cm⁻¹, which is a superposition of several bands of the O–H stretching modes of molecular water and silanol [41,43]. The sharp narrow peak at 3742 cm⁻¹ (Fig. 4b) can be assigned to the stretching vibrations of the SiO–H bond [43]. The peaks at 2800–3000 cm⁻¹ are typical of detonation nanodiamonds and relate to the stretching vibrations of the CH bond in the CH₂ and CH₃ defect groups [44,45].

The middle panels in Fig. 4a and b depict the IR spectrum of the compacted composite. The peaks in the range of 400–2100 cm⁻¹ belong to the stretching/bending vibrations of the SiO₄ tetrahedron and weak second-order silicate overtones of crystalline coesite formed from the initially amorphous SiO₂ aerogel. The spectrum generally agrees with all experimental data from previous studies [46]. The intensity of the 3362 cm⁻¹ peak of the O–H stretching vibrations decreased about fivefold compared to the initial aerogel (Fig. 4b). This indicates a decrease in the content of hydroxyl groups and water after the compaction and crystallization of the sample. The peak due to the H–O–H bending vibrations of water molecules adsorbed by the compacted composite is observed at

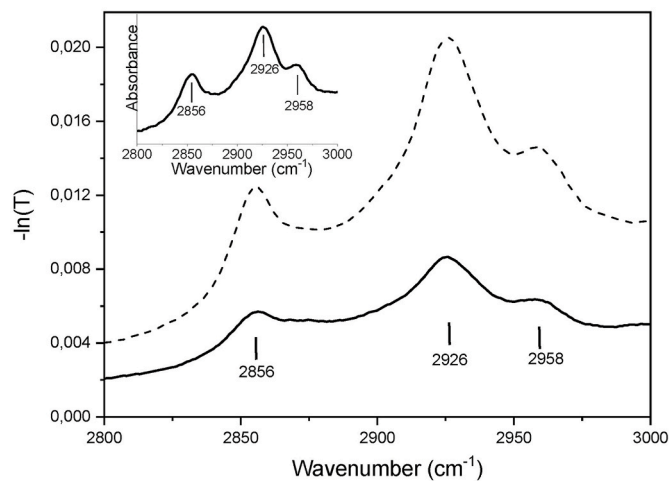


Fig. 5. Infrared spectra of stretching vibrations of CH₂ and CH₃ groups in the DNDs/SiO₂ composite compacted (dashed black curve) and then hydrogenated (solid black curve) at a pressure of 7.5 GPa (data from Fig. 4). The integral intensities of the peaks are normalized to the intensity of the coesite peak at 1086–1103 cm⁻¹. The inset shows the IR spectrum of a sample consisting of individual nanodiamonds.

1598 cm⁻¹ near the set of silicate overtones of crystalline coesite at 1653, 1728, 1858, 1955, and 1993 cm⁻¹ (peaks a–e in Fig. 7 [46]).

No peaks characteristic of SiC crystals or Si–C bonds were observed either in the X-ray diffraction patterns or in the IR spectra. Thus, the carbon shells of nanodiamonds did not react with silicon of the SiO₂ matrix, and the compression of the aerogel with nanodiamonds to 7.5 GPa at 250 °C resulted in the formation of a composite of individual phases of DNDs and SiO₂.

The IR spectroscopy showed that the light absorption due to the O–H stretching vibrations excited in the hydrogenated sample decreased by two times compared to the compacted sample and by sixteen times compared to the initial aerogel. After the hydrogenation, the intensity of the peak of the H–O–H bending vibrations of water molecules also decreased by 1.5 times. The marked reduction in the content of water and hydroxyl groups in the compacted and hydrogenated samples was likely a consequence of the decrease in their specific surface area after the exposure under an external pressure of 7.5 GPa at an elevated temperature of 250 °C in an inert medium and then at 600 °C in a hydrogen atmosphere. Due to the small total amount of water and

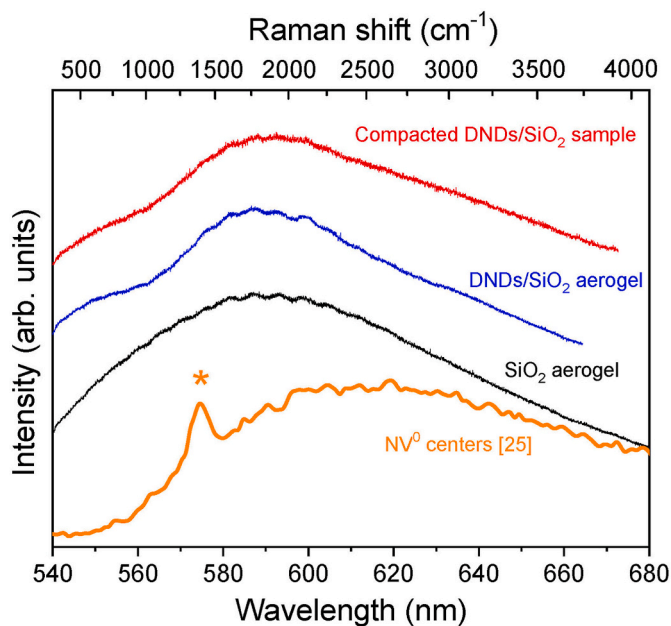


Fig. 6. Photoluminescence spectra of SiO₂ aerogel without nanodiamonds (black curve) and the initial SiO₂ aerogel containing 6 wt% DNDs (blue curve) and this aerogel compacted at 7.5 GPa and 250 °C (red curve). The orange curve at the bottom of the Figure shows the photoluminescent spectrum of NV⁰ centers in nanodiamonds measured in Ref. [25]. The orange asterisk indicates the position of the zero-phonon peak. (For interpretation of the references to color in this figure legend, the reader is referred to the Web version of this article.)

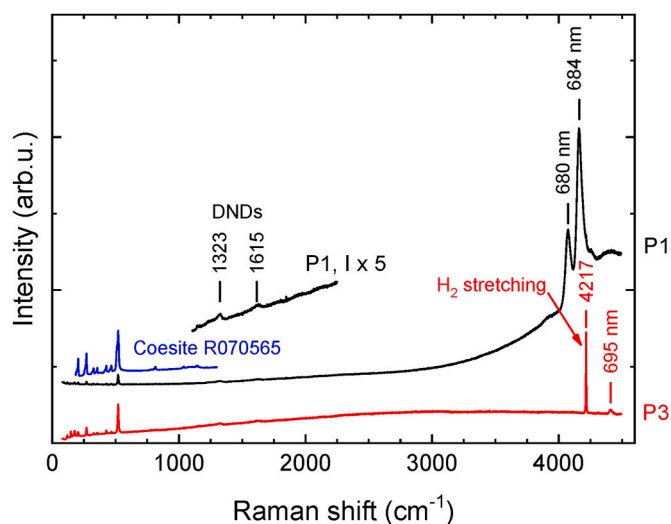


Fig. 7. Raman spectra of the SiO₂ aerogel – nanodiamonds composite subjected to high hydrogen pressure of 7.5 GPa and 600 °C. The spectra were acquired from two representative points on the sample surface labeled as P1 and P3. Above the experimental spectra (black and red curves), the spectrum of the coesite phase of silica from the RRUFF database (<https://rruff.info>; R070565, blue curve) is shown. The part of the P1 spectrum in the frequency range corresponding to nanodiamonds was multiplied by a factor of 5 in order to demonstrate the weak peaks of the nanodiamond grains embedded in the SiO₂ matrix. The positions of the Raman peaks are indicated by vertical bars with frequency values (in cm⁻¹) above them. In the high frequency range of the spectra (above 3000 cm⁻¹), relatively broad luminescence peaks are observed. The positions of their maxima are given in nanometers. (For interpretation of the references to color in this figure legend, the reader is referred to the Web version of this article.)

hydroxyl groups released from the samples, we were unable to determine where they went in the reaction cell.

In the IR spectrum of the hydrogenated sample, the intensity of the 2856, 2926, and 2958 cm⁻¹ peaks corresponding to the stretching vibrations of C–H bonds in the CH₂ and CH₃ groups, decreased almost twofold compared to the compacted sample (Fig. 5 shows these peaks on an enlarged scale; the inset shows the spectrum of individual nanodiamonds outside the SiO₂ matrix). This may indicate a decrease in the size of the sp² shell of nanodiamonds, where the CH₂ and CH₃ groups were located. However, to assess the change in the fraction of the sp² shell of a nanodiamond relative to its sp³ core, Raman data are needed, since the stretching vibration mode of sp³ carbon is inactive in the infrared range.

3.3. Raman spectroscopy

As seen from Fig. 6, the investigation of SiO₂ aerogel without nanodiamonds only yielded an intense and almost featureless spectrum with a maximum at 1800–1900 cm⁻¹ caused by photoluminescence of dangling Si–O bonds and other defects [23]. The SiO₂ luminescence also masked all Raman peaks in the spectra of the initial and compacted aerogel with DNDs. The upper two spectra looked similar to each other and differed from the spectrum of pure aerogel by the presence of something like a modulation to the left of the maximum. The modulation could result from the luminescence of NV⁰ centers in the DNDs (see an experimental NV⁰ spectrum [25] at the bottom of the figure).

After further hydrogenation of the compacted DNDs/SiO₂ sample at 7.5 GPa and 600 °C, the luminescent background was drastically reduced and Raman peaks appeared. Fig. 7 shows a general view of the Raman spectra of the hydrogenated DNDs/SiO₂ composite collected at different points on the sample surface.

As one can see from Fig. 7, all spectra have a set of narrow Raman peaks of crystalline coesite in the frequency range of 200–550 cm⁻¹, peaks of “sp³ core” carbon at 1323 cm⁻¹ and “sp² surf.” carbon at 1615 cm⁻¹, as well as peaks of stretching vibrations of molecular hydrogen at 4217 cm⁻¹. The frequency of the narrow peak of stretching vibrations significantly exceeds the frequency of 4140 cm⁻¹ of this vibrational mode in H₂ gas at atmospheric pressure. In fact, the frequency of 4217 cm⁻¹ corresponds to a hydrogen gas compressed to 7.5 GPa [47], which was the hydrogenation pressure of the sample.

Additionally, some spectra contained two broad and intense peaks at 4070 and 4157 cm⁻¹, overlapping with a very broad band with a maximum at the Raman shift frequency of ~4400 cm⁻¹. These features could not be due to the hydrogen dissolved in the sample since its content H₂/SiO₂ = 0.005 was too low.

The luminescence of NV⁻ centers in bulk CVD diamond is known to produce a zero-phonon line with a wavelength λ = 637 nm or a Raman shift of 3098 cm⁻¹ [48–50]. However, in DNDs, the intensity of this line is high only at temperatures below 80 K. With increasing temperature, its intensity decreases significantly and drops to several percent of the total luminescence intensity of NV⁻ centers at room temperature [4]. Moreover, the zero-phonon line near 637 nm is often not resolved in the spectra of nanodiamonds containing NV⁻ centers [51,52]. A complete absence of the zero-phonon line was also observed for individual DNDs lying freely on a substrate or embedded into polymers [51]. According to Ref. [53], this could occur due to a change in the position of excited/ground states in the band gap for NV⁻ centers lying near the surface of the particle, and the subsequent broadening of the spectral components of the 637 nm zero-phonon line for ensembles of such NV⁻ centers with slightly different electronic parameters.

At room temperature, the largest contribution to luminescence comes from a broad phonon band with λ = 630–800 nm and maximum intensity at a wavelength of ~690 nm (4300 cm⁻¹) [4]. The formation of this band is due to the Franck-Condon effect and the increasing probability of the electron-phonon transition with increasing temperature. Thus, the most likely origin of the broad band observed in this study

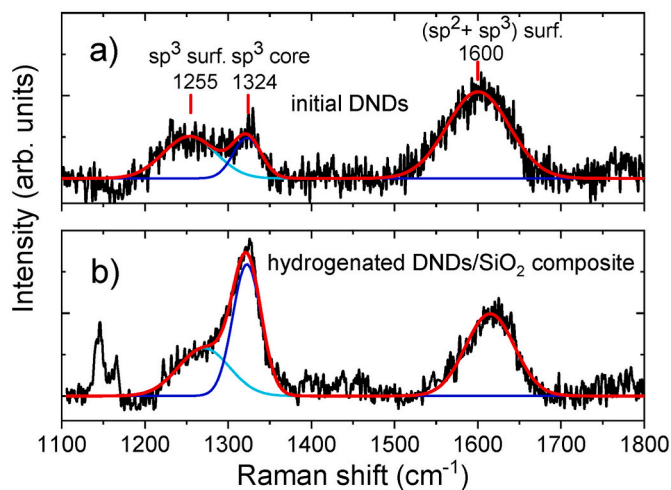


Fig. 8. Raman spectra of (a) the initial nanodiamonds and (b) bulk DNDs/SiO₂ composite with 6 wt% DNDs hydrogenated at P = 7.5 GPa and T = 600 °C. The black curves show the experimental dependencies with the background subtracted. The cyan and blue curves represent the Gaussian decomposition of the spectra. The red curves depict the envelopes of the sums of all Gaussians. (For interpretation of the references to color in this figure legend, the reader is referred to the Web version of this article.)

with an intensity maximum at ~ 4400 cm⁻¹ or $\lambda \sim 695$ nm (upper scale in Fig. 7) is the photoluminescence of NV⁻ centers in the nanodiamonds. The fact that this line belongs to the phonon luminescence band of NV⁻ centers in nanodiamond is further confirmed by the difference of 1302 cm⁻¹ between the Raman frequencies of the zero-phonon line (3098 cm⁻¹) and its intensity maximum (4400 cm⁻¹), which approximately corresponds to the Raman shift of the “sp³ core” of the DND at ≈ 1324 cm⁻¹.

The origin of the peaks at 4070 and 4157 cm⁻¹ is unclear. Among other things, these could be the luminescence at $\lambda = 679$ and 683 nm of impurity chromium cations [54] that diffused into the surface layer of the silica matrix from the alundum crucible used to anneal the initial DNDs/SiO₂ aerogel in air at 400 °C. This assignment is corroborated by the presence of a luminescent peak at $\lambda = 695$ nm from an aluminum impurity [55], apparently diffused from the alundum crucible.

Fig. 8 compares Raman spectra of the nanodiamonds used to prepare the initial aerogel (a) and the hydrogenated DNDs/SiO₂ composite with 6 wt% DNDs (b). The spectra consist of overlapping peaks “sp³ surf.” at ≈ 1255 cm⁻¹ and “sp³ core” at ≈ 1324 cm⁻¹, which can roughly be resolved using Gaussians, and of unresolved peaks “sp² surf.” and “sp³ surf.” at ≈ 1600 cm⁻¹. The designations “surf.” and “core” refer, respectively, to the carbon in the surface layer and deep inside the nanodiamonds. The peaks are classified according to Refs. [56,57]. As one can see, the relative intensity of the “sp³ core” peak increases significantly after the hydrogenation of the sample. Namely, the ratio of the integral intensities of the overlapping “sp³ core” and “sp³ surf.” peaks increases by 3.9 times, and the ratio of the intensity of the “sp³ core” peak to the intensity of all peaks increases by 3.4 times. This suggests that the hydrogenation strongly reduced the amount of both sp³ and sp² surface carbon in the nanodiamonds.

The width of the peaks in the Raman spectrum of the hydrogenated DNDs/SiO₂ composite with 6 wt% DNDs corresponds to the nanodiamond size of 6–8 nm [56,58] in agreement with the results of X-ray diffraction (Section 3.1) and the results of transmission electron microscopy for the original DNDs hydrosol [20]. Thus, we conclude that the thermobaric treatment of the initial DNDs/SiO₂ aerogel did not lead to agglomeration of the embedded nanodiamonds.

4. Discussion

X-ray diffraction, IR and Raman spectroscopy revealed no traces of Si or SiC in the samples of compacted and hydrogenated DNDs/SiO₂ composite. This indicates the absence of possible reactions [31] of silica and carbon at a pressure of 7.5 GPa and temperatures up to 600 °C. That is, within the sensitivity of the methods used, carbon in the hydrogenated DNDs/SiO₂ composite is only contained in individual diamond nanocrystals separated from the silica matrix.

X-ray diffraction also showed that the compaction of the DNDs/SiO₂ aerogel at 7.5 GPa and 250 °C resulted in crystallization of its amorphous SiO₂ matrix into the high-pressure coesite phase (see Fig. 3). This is an undesirable effect because crystalline coesite is less optically transparent than amorphous SiO₂. The formation of coesite from silica glass at pressures of 3.5–6.0 GPa usually requires a higher temperature of 500–1200 °C [59]. The temperatures of crystallization of silica glass [35] and silica gel [60] into coesite become much lower, down to 190 °C, due to the presence of hydroxyl groups –OH in the material. In view of the large specific surface area, our initial aerogel contained many hydroxyl –OH groups (see Fig. 4) despite its preliminary annealing in air at 400 °C.

Note in this regard that preventing crystallization of the silica matrix is only a problem of the primary compaction of DNDs/SiO₂ aerogel under quasi-hydrostatic pressure. Our previous experiments showed that amorphous SiO₂ samples with different specific surface areas never crystallized under compression in an H₂ atmosphere to 7.5 GPa and temperatures up to 280 °C [28,61,62]. Moreover, the hydrogenated silica glass never experienced irreversible densification [61] characteristic of amorphous SiO₂ compressed in an inert medium [59].

As seen from the spectra in Fig. 7, the hydrogenation of the compacted DNDs/SiO₂ composite effectively suppressed photoluminescence of the SiO₂ matrix at wavelengths up to $\lambda \sim 640$ nm and even higher (most likely, due to the passivation of dangling Si–O bonds and other defects). The broad luminescence band of NV⁰ centers inherent in DNDs also disappeared (this band with a maximum intensity at $\lambda \sim 620$ nm [25] is shown by the orange curve at the bottom of Fig. 6). Instead of the NV⁰ band, Fig. 7 demonstrates another broad and intense luminescence band with a maximum at $\lambda \sim 695$ nm, which was observed at some points (P1 and P2) on the surface of the hydrogenated sample. We believe it is the luminescence of negatively charged NV⁻ centers formed from the neutral NV⁰ centers owing to the partial removal of electron traps located predominantly in the highly disordered surface layer of the nanodiamonds. This effect was observed and examined in the work of Ref. [25], where the authors used oxidation to remove the amorphous shell from nanodiamonds.

In Ref. [25], the shell around the nanodiamonds was considered to consist of sp²-hybridized carbon. However, according to recent studies [56,63], the shell is mainly formed from sp³-bonded carbon. In particular, the Raman peak at ~ 1600 cm⁻¹ in Fig. 8, which was previously attributed entirely to the sp²-bonded surface carbon [57], is primarily due to the sp³ carbon. Thus, the changes in the Raman spectra caused by the hydrogenation (compare Fig. 7a and b) do not allow us to estimate the accompanying changes in the ratio of the amount of sp³- and sp²-hybridized carbon covering the nanodiamonds. These changes also cannot be determined from the IR spectra shown in Fig. 4. What can be said with confidence is that the hydrogenation greatly reduces the total amount of the sp²+sp³ surface carbon compared to the sp³ carbon inside the nanodiamonds. This directly follows from the Raman spectra in Fig. 8 and agrees with the IR spectra in Fig. 5, which demonstrate a strong decrease in the intensity of peaks of the stretching vibrations of CH₂ and CH₃ groups located in the disordered shells of nanodiamonds.

The hydrogenation could only reduce the disordered shells of nanodiamonds if they reacted with hydrogen diffused to them through the SiO₂ matrix. The question arises as to what compounds are formed in this reaction. There are at least two different scenarios possible. One of them is the formation of multilayer graphane (hydride of graphite), an

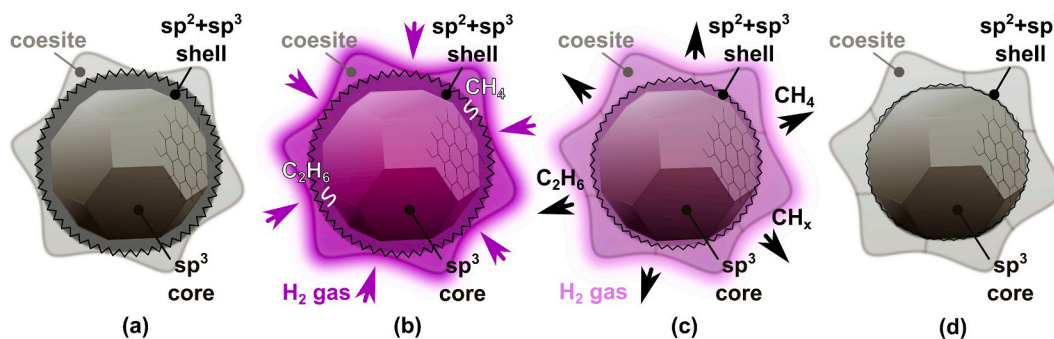


Fig. 9. Removing the disordered carbon from the surface of DNDs: (a) Bulk DNDs/SiO₂ composite produced at 7.5 GPa and 250 °C in an inert medium; (b) Diffusion of H₂ molecules through the SiO₂ matrix at an external hydrogen pressure of 7.5 GPa and a temperature of 600 °C and their reaction with the sp²+sp³ shell of DNDs resulting in the formation of light hydrocarbons; (c) Release of light hydrocarbons from the composite during the decrease in pressure at room temperature, accompanied by thinning of the sp²+sp³ shell of nanodiamonds. (d) Bulk DNDs/SiO₂ composite, in which the sp²+sp³ shell of nanodiamonds is partially removed by the hydrogen treatment at high pressure.

optically transparent sp³-bonded crystalline dielectric compound with CH stoichiometry, which can be synthesized from ball-milled graphite powder and gaseous hydrogen at pressures above 2 GPa and temperatures from 450 to 700 °C [33]. This scenario did not materialize, as the strongest peak at 2680 cm⁻¹ of graphite hydride [33] was not observed in any IR spectrum of the hydrogenated DNDs/SiO₂ sample (see Fig. 7).

Another scenario for the disappearance of most of the disordered carbon from the surface of nanodiamonds is the hypothetical formation of light hydrocarbons, such as methane CH₄ and ethane C₂H₆, which should be thermodynamically stable phases under the hydrogenation conditions [64]. No features characteristic of these compounds was detected in the IR (Fig. 4) and Raman (Fig. 7) spectra of the hydrogenated DNDs/SiO₂ sample, but a plausible explanation can be found for this. Namely, the light hydrocarbons are volatile under normal conditions. In contrast to the solid multilayer graphane, they could have been released from the hydrogenated sample when the pressure was lowered before the spectroscopic measurements (see Fig. 9), therefore leaving no fingerprints in the IR and Raman spectra.

The rapid release of methane and ethane from the sample appears realistic, since the diffusion coefficient of these compounds in silicates increases by several orders of magnitude with decreasing pressure [65].

Thus, as a result of hydrogenation at a pressure of 7.5 GPa of the preformed DNDs/SiO₂ composite, we obtained a massive dense sample of optically transparent silicon dioxide with uniformly distributed individual nanodiamonds protected against many gases and demonstrating NV⁻ luminescence at room temperature. The luminescence of individual nanodiamonds enclosed in an optically transparent and chemically resistant shell is necessary for the creation of single-photon emitters for quantum applications [10] and temperature sensors capable of operating over a wide temperature range in reactive gases [19]. The compacted composite obtained in our work can obviously be used for these purposes after grinding to DND/SiO₂ particles of the size required for coatings or suspensions.

5. Conclusions

High-pressure treatment of SiO₂ aerogel with 6 wt% nanodiamonds produced a new composite material consisting of individual DNDs uniformly distributed over the volume of a dense SiO₂ matrix protecting them from agglomeration and chemical interaction with the environment. Further high-pressure treatment in a hydrogen atmosphere eliminated the intense luminescence of the matrix and made it optically transparent. Due to the hydrogenation, a significant portion of the disordered carbon shell containing electron traps was also removed from the surface of the nanodiamonds. This converted the neutral NV⁰ centers “impurity nitrogen atom – vacancy” inside the nanodiamonds into negatively charged NV⁻ centers. As a result, the luminescence of NV⁰

centers typical of nanodiamonds at room temperature was replaced by the luminescence of NV⁻ centers, which is much more suitable for applications. Currently, DNDs are the only type of nanodiamonds that can be produced on an industrial scale, and the composite obtained in this work is the first material that allows the use of the luminescence of their NV⁻ centers.

CRediT authorship contribution statement

M.A. Korotkova: Writing – original draft, Investigation. **V.S. Efimchenko:** Writing – review & editing, Investigation, Conceptualization. **V.E. Antonov:** Writing – review & editing, Validation, Supervision, Investigation. **O.I. Barkalov:** Writing – review & editing, Methodology, Investigation. **I.G. Fomina:** Writing – review & editing, Validation, Resources. **T.N. Fursova:** Writing – review & editing, Methodology, Investigation. **K.A. Gavrilicheva:** Investigation. **S.V. Zaitsev:** Methodology, Investigation. **I.O. Gozhikova:** Resources, Investigation. **A.Ya. Vul’:** Validation, Resources. **S.A. Lermontov:** Writing – review & editing, Resources, Investigation, Conceptualization.

Declaration of competing interest

The authors declare that they have no known competing financial interests or personal relationships that could have appeared to influence the work reported in this paper.

Acknowledgements

This work was supported by the Ministry of Science and Higher Education of the Russian Federation as part of the State Assignments of the Osipyan Institute of Solid State Physics of the Russian Academy of Sciences (ISSP RAS) and of the Kurnakov Institute of General and Inorganic Chemistry of the Russian Academy of Sciences (IGIS RAS) and of the Institute of Physiologically Active Compounds at Federal Research Center of Problems of Chemical Physics and Medicinal Chemistry of the Russian Academy of Sciences (IPAC RAS, theme FFSG-2024-0019).

The authors acknowledge Dr. Vladimir Fedotov (ISSP RAS) for the X-ray diffraction measurements.

References

- [1] D.M. Gruen, O.A. Shenderova, A.Ya. Vul’ (Eds.), *Synthesis, Properties and Applications of Ultrananocrystalline Diamond*, first ed., Springer, Dordrecht, 2005 <https://doi.org/10.1007/1-4020-3322-2>.
- [2] J.-C. Arnault (Ed.), *Nanodiamonds: Advanced Material Analysis, Properties and Applications*, first ed., Elsevier, 2017 <https://doi.org/10.1016/C2015-0-01721-X>.
- [3] F. Pan, M. Khan, A.H. Ragab, E. Javed, H.A. Alsalmah, I. Khan, T. Lei, A. Hussain, A. Mohamed, A. Zada, M.Z. Ansari, Recent advances in the structure and

- biomedical applications of nanodiamonds and their future perspectives, *Mater. Des.* 233 (2023) 112179, <https://doi.org/10.1016/j.matdes.2023.112179>.
- [4] R. Schirhagl, K. Chang, M. Loretz, C.L. Degen, Nitrogen-vacancy centers in diamond: nanoscale sensors for physics and biology, *Annu. Rev. Phys. Chem.* 65 (2014) 83–105, <https://doi.org/10.1146/annurev-physchem-040513-103659>.
- [5] V. Sonin, A. Tomilenko, E. Zhimulev, T. Bul'bak, A. Chepurov, Y. Babich, A. Logvinova, T. Timina, A. Chepurov, The composition of the fluid phase in inclusions in synthetic HPHT diamonds grown in system Fe–Ni–Ti–C, *Sci. Rep.* 12 (2022) 1246, <https://doi.org/10.1038/s41598-022-05153-7>.
- [6] F.C. Waldermann, P. Olivero, J. Nunn, K. Surmacz, Z.Y. Wang, D. Jaksch, R. A. Taylor, I.A. Walmsley, M. Draganski, P. Reichart, A.D. Greentree, D. N. Jamieson, S. Praver, Creating diamond color centers for quantum optical applications, *Diam. Relat. Mater.* 16 (2007) 1887–1895, <https://doi.org/10.1016/j.diamond.2007.09.009>.
- [7] V.M. Acosta, E. Bauch, M.P. Ledbetter, C. Santori, K.-M.C. Fu, P.E. Barclay, R. G. Beausoleil, H. Linet, J.F. Roch, F. Treussart, S. Chemsisour, W. Gawlik, D. Budker, Diamonds with a high density of nitrogen-vacancy centers for magnetometry applications, *Phys. Rev. B* 80 (2009) 115202, <https://doi.org/10.1103/PhysRevB.80.115202>.
- [8] V.N. Mochalin, O. Shenderova, D. Ho, Y. Gogotsi, The properties and applications of nanodiamonds, *Nat. Nanotechnol.* 7 (2012) 11–23, <https://doi.org/10.1038/nnano.2011.209>.
- [9] J.P. Boudou, P.A. Curmi, F. Jelezko, J. Wrachtrup, P. Aubert, M. Sennour, G. Balasubramanian, R. Reuter, A. Thorel, E. Gaffet, High yield fabrication of fluorescent nanodiamonds, *Nanotechnology* 20 (2009) 235602, <https://doi.org/10.1088/0957-4484/20/23/235602>.
- [10] I.I. Vlasov, E.A. Ekimov, O.S. Kudryatsev, O.A. Shenderova, M. Metsch, F. Jelezko, Luminescent nanodiamonds as a material platform for production of single photon emitters, *J. Phys.: Conf. Ser.* 1092 (2018) 012160, <https://doi.org/10.1088/1742-6596/1092/1/012160>.
- [11] V.Yu. Dolmatov, A.N. Ozerin, I.I. Kulakova, O.O. Bochechka, N.M. Lapchuk, V. Myllymäki, A. Vehanen, Detonation nanodiamonds: new aspects in the theory and practice of synthesis, properties and applications, *Russ. Chem. Rev.* 89 (2020) 1428, <https://doi.org/10.1070/rcr4924>.
- [12] A. Krüger, F. Kataoka, M. Ozawa, T. Fujino, Y. Suzuki, A.E. Aleksenskii, A.Ya. Vul', E. Osawa, Unusually tight aggregation in detonation nanodiamond: identification and disintegration, *Carbon* 43 (2005) 1722–1730, <https://doi.org/10.1016/j.carbon.2005.02.020>.
- [13] A.T. Dideikin, A.E. Aleksenskii, M.V. Baidakova, P.N. Brunkov, M. Brzhezinskaya, V.Yu. Davydov, V.S. Levitskii, S.V. Kidalov, Yu.A. Kukushkina, D.A. Kirilenko, V. V. Shnitov, A.V. Shvidchenko, B.V. Senkovskiy, M.S. Shestakov, A.Ya. Vul', Rehybridization of carbon on facets of detonation diamond nanocrystals and forming hydrosols of individual particles, *Carbon* 122 (2017) 737–745, <https://doi.org/10.1016/j.carbon.2017.07.013>.
- [14] A. Kume, V.N. Mochalin, Sonication-assisted hydrolysis of ozone oxidized detonation nanodiamond, *Diam. Relat. Mater.* 103 (2020) 107705, <https://doi.org/10.1016/j.diamond.2020.107705>.
- [15] N. Nunn, M. Torelli, G. McGuire, O. Shenderova, Nanodiamond: high impact nanomaterial, *Curr. Opin. Solid State Mater. Sci.* 21 (2017) 1–9, <https://doi.org/10.1016/j.cossms.2016.06.008>.
- [16] S.V. Koniakhin, M.K. Rabchinskii, N.A. Besedina, L.V. Sharonova, A. V. Shvidchenko, E.D. Eidelman, Evidence of absorption dominating over scattering in light attenuation by nanodiamonds, *Phys. Rev. Res.* 2 (2020) 013316, <https://doi.org/10.1103/PhysRevResearch.2.013316>.
- [17] M.D. Torelli, N.A. Nunn, O.A. Shenderova, A perspective on fluorescent nanodiamond bioimaging, *Small* 15 (2019) 1902151, <https://doi.org/10.1002/smll.201902151>.
- [18] R. Khoz, F. Yazdian, M. Pourmadadi, A. Rahdar, S. Fathi-karkan, S. Pandey, Current trends in silica based drug delivery systems, *Eur. J. Med. Chem. Rep.* 12 (2024) 100206, <https://doi.org/10.1016/j.ejmc.2024.100206>.
- [19] X. Jing, Y. Xu, H. Gan, P. Hu, C. Li, J. Qian, J. Zhang, Y. Tian, S. Xu, Synthesis and fluorescent thermal response of sol-gel SiO₂ composite film containing nanodiamonds, *Carbon* 184 (2021) 303–311, <https://doi.org/10.1016/j.carbon.2021.08.038>.
- [20] I.G. Fomina, N.A. Sipyagina, E.A. Straumal, G.P. Kopitsa, A.A. Mazilkin, A. A. Eliseev, N.N. Efimov, Y.S. Zavorotny, A.V. Shvidchenko, A.Ya. Vul', I. L. Eremenko, S.A. Lermontov, First example of single-crystal nanodiamonds immobilized in porous SiO₂-aerogel matrix: synthesis and characterization, *ChemNanoMat* 10 (2024) 202400172, <https://doi.org/10.1002/cnma.202400172>.
- [21] B. Zhou, J. Shen, Y. Wu, G. Wu, X. Ni, Hydrophobic silica aerogels derived from polyethoxydisiloxane and perfluoroalkylsilane, *Mater. Sci. Eng. C* 27 (2007) 1291–1294, <https://doi.org/10.1016/j.msec.2006.06.032>.
- [22] A. Ayral, J. Phalippou, T. Woignier, Skeletal density of silica aerogels determined by helium pycnometry, *J. Mater. Sci.* 27 (1992) 1166–1170, <https://doi.org/10.1007/BF01142014>.
- [23] I.I. Hinić, G.M. Stanišić, Z.V. Popović, Photoluminescence properties of silica aerogel during sintering process, *J. Sol. Gel Sci. Technol.* 14 (1999) 281–289, <https://doi.org/10.1023/A:1008721613490>.
- [24] J. Ristein, Electronic properties of diamond surfaces – blessing or curse for devices? *Diam. Relat. Mater.* 9 (2000) 1129–1137, [https://doi.org/10.1016/S0925-9635\(99\)00316-7](https://doi.org/10.1016/S0925-9635(99)00316-7).
- [25] L. Rondin, G. Dantelle, A. Slablab, F. Grosshans, F. Treussart, P. Bergonzo, S. Perruchas, T. Gacoin, M. Chaigneau, H.-C. Chang, V. Jacques, J.-F. Roch, Surface-induced charge state conversion of nitrogen-vacancy defects in nanodiamonds, *Phys. Rev. B* 82 (2010) 115449, <https://doi.org/10.1103/PhysRevB.82.115449>.
- [26] A.E. Aleksenskii, M.V. Baidakova, A.Ya. Vul', A.T. Dideikin, V.I. Siklitskii, S.P. Vul', Effect of hydrogen on the structure of ultradisperse diamond, *Phys. Solid State* 42 (2000) 1575–1578, <https://doi.org/10.1134/1.1307073>.
- [27] A.M. Panich, A.E. Aleksenskii, Deaggregation of diamond nanoparticles studied by NMR, *Diam. Relat. Mater.* 27–28 (2012) 45–48, <https://doi.org/10.1016/j.diamond.2012.05.005>.
- [28] K.P. Meletov, V.S. Efimchenko, Stability of hydrogenated silica glass and desorption kinetics of molecular hydrogen, *Chem. Phys. Lett.* 793 (2022) 139477, <https://doi.org/10.1016/j.cplett.2022.139477>.
- [29] C.M. Hartwig, Raman scattering from hydrogen and deuterium dissolved in silica as a function of pressure, *J. Appl. Phys.* 47 (1976) 956–959, <https://doi.org/10.1063/1.322686>.
- [30] J. Qian, C. Pantea, J. Huang, T.W. Zerda, Y. Zhao, Graphitization of diamond powders of different sizes at high pressure–high temperature, *Carbon* 42 (2004) 2691–2697, <https://doi.org/10.1016/j.carbon.2004.06.017>.
- [31] B. Abolpour, R. Shamsoddini, Mechanism of reaction of silica and carbon for producing silicon carbide, *Prog. React. Kinet. Mech.* 45 (2019) 1468678319891416, <https://doi.org/10.1177/1468678319891416>.
- [32] A. Shinozaki, H. Kagi, N. Noguchi, H. Hirai, H. Ohfui, T. Okada, S. Nakano, T. Yagi, Formation of SiH₄ and H₂O by the dissolution of quartz in H₂ fluid under high pressure and temperature, *Am. Mineral.* 99 (2014) 1265–1269, <https://doi.org/10.2138/am.2014.4798>.
- [33] V.E. Antonov, I.O. Bashkin, A.V. Bazhenov, B.M. Bulychev, V.K. Fedotov, T. N. Fursova, A.I. Kolesnikov, V.I. Kulakov, R.V. Lukashev, D.V. Matveev, M. K. Sakharov, Y.M. Shulga, Multilayer graphene synthesized under high hydrogen pressure, *Carbon* 100 (2016) 465–473, <https://doi.org/10.1016/j.carbon.2015.12.051>.
- [34] A.E. Aleksenskii, E.D. Eydelman, A.Ya. Vul', Deagglomeration of detonation nanodiamonds, *Nanosci. Nanotechnol. Lett.* 3 (2011) 68–74, <https://doi.org/10.1166/nml.2011.1122>.
- [35] G.-Q. Zhang, D.-P. Xu, G.-X. Song, Y.-F. Xue, L. Li, D.-Y. Wang, W.-H. Su, Effect of Si-OH on the transformation of amorphous SiO₂ to coesite, *J. Alloys Compd.* 476 (2009) L4–L7, <https://doi.org/10.1016/j.jallcom.2008.08.049>.
- [36] E.B. Yudina, P.A. Romanov, A.S. Chizhikova, N.N. Aruev, Pyrolysis mass-spectrometry study of detonation nanodiamonds surface chemistry, Fullerenes, Nanotub. Carbon Nanostruct. 31 (2023) 68–74, <https://doi.org/10.1080/1536383X.2022.2120477>.
- [37] L.G. Khvostantsev, V.N. Slesarev, V.V. Brazhkin, Toroid type high-pressure device: history and prospects, *High Press. Res.* 24 (2004) 371–383, <https://doi.org/10.1080/08957950412331298761>.
- [38] V.E. Antonov, B.M. Bulychev, V.K. Fedotov, D.I. Kapustin, V.I. Kulakov, I.A. Sholin, NH₃BH₃ as an internal hydrogen source for high pressure experiments, *Int. J. Hydrogen Energy* 42 (2017) 22454–22459, <https://doi.org/10.1016/j.ijhydene.2017.03.121>.
- [39] L.H. Cohen, W. Klement, High-low quartz inversion: determination to 35 kilobars, *J. Geophys. Res.* 72 (1967) 4245–4251, <https://doi.org/10.1029/jz072i016p04245>.
- [40] C.T. Kirk, Quantitative analysis of the effect of disorder-induced mode coupling on infrared absorption in silica, *Phys. Rev. B* 38 (1988) 1255–1273, <https://doi.org/10.1103/PhysRevB.38.1255>.
- [41] R. Al-Oweini, H. El-Rassy, Synthesis and characterization by FTIR spectroscopy of silica aerogels prepared using several Si(OR)₄ and R'³Si(OR)₃ precursors, *J. Mol. Struct.* 919 (2009) 140–145, <https://doi.org/10.1016/j.jmolstruc.2008.08.025>.
- [42] H.A. Benesi, A.C. Jones, An infrared study of the water-silica gel system, *J. Phys. Chem.* 63 (1959) 179–182, <https://doi.org/10.1021/j150572a012>.
- [43] P. Innocenzi, Infrared spectroscopy of sol-gel derived silica-based films: a spectro-structure overview, *J. Non-Cryst. Solids* 316 (2003) 309–319, [https://doi.org/10.1016/S0022-3093\(02\)01637-X](https://doi.org/10.1016/S0022-3093(02)01637-X).
- [44] V.L. Kuznetsov, Y.V. Butenko, 13 - diamond phase transitions at nanoscale, in: O. A. Shenderova, D.M. Gruen (Eds.), *Ultrananocrystalline Diamond: Synthesis, Properties, and Applications*, William Andrew Publishing, Norwich, NY, 2006, pp. 405–475, <https://doi.org/10.1016/B978-081551524-1.50015-9>.
- [45] T. Petit, L. Puskar, FTIR spectroscopy of nanodiamonds: methods and interpretation, *Diam. Relat. Mater.* 89 (2018) 52–66, <https://doi.org/10.1016/j.diamond.2018.08.005>.
- [46] X. Liu, Y. Ma, Q. He, M. He, Some IR features of SiO₄ and OH in coesite, and its amorphization and dehydration at ambient pressure, *J. Asian Earth Sci.* 148 (2017) 315–323, <https://doi.org/10.1016/j.jseas.2017.03.016>.
- [47] W. Xu, X.-D. Liu, M. Peña-Alvarez, H.-C. Jiang, P. Dalladay-Simpson, B. Coasne, J. Haines, E. Gregoryanz, M. Santoro, High-pressure insertion of dense H₂ into a model zeolite, *J. Phys. Chem. C* 125 (2021) 7511–7517, <https://doi.org/10.1021/acs.jpcc.1c02177>.
- [48] Z. Guo, X. Zhu, K. Wang, Y. Zhang, Y. Tian, H. Wang, Influence of near threshold energy electron irradiation on the thermal conductivity of IIa diamond, *Appl. Phys. Lett.* 119 (2021) 182105, <https://doi.org/10.1063/5.0067003>.
- [49] R. Guo, K. Wang, Y. Zhang, Z. Xiao, G. Jia, H. Wang, Y. Wu, Y. Tian, Adjustable charge states of nitrogen-vacancy centers in low-nitrogen diamond after electron irradiation and subsequent annealing, *Appl. Phys. Lett.* 117 (2020) 172104, <https://doi.org/10.1063/5.0023369>.
- [50] K. Wang, J.W. Steeds, A. Sarua, Inhomogeneity distribution of impurities in high temperature high pressure synthesized boron-doped diamond, *Diam. Relat. Mater.* 130 (2022) 109540, <https://doi.org/10.1016/j.diamond.2022.109540>.
- [51] C. Bradac, T. Gaebel, N. Naidoo, M.J. Sellars, J. Twamley, L.J. Brown, A.S. Barnard, T. Plakhotnik, A.V. Zvyagin, J.R. Rabeau, Observation and control of blinking nitrogen-vacancy centres in discrete nanodiamonds, *Nat. Nanotechnol.* 5 (2010) 345–349, <https://doi.org/10.1038/nnano.2010.56>.

- [52] S.K.H. Andersen, S. Kumar, S.I. Bozhevolnyi, Coupling of nitrogen-vacancy centers in a nanodiamond to a silver nanocube, *Opt. Mater. Express* 6 (2016) 3394–3406, <https://doi.org/10.1364/ome.6.003394>.
- [53] V.Yu. Osipov, F. Treussart, S.A. Zargaleh, K. Takai, F.M. Shakhov, B.T. Hogan, A. Baldycheva, Photoluminescence from NV⁻ centres in 5 nm detonation nanodiamonds: identification and high sensitivity to magnetic field, *Nanoscale Res. Lett.* 14 (2019) 279, <https://doi.org/10.1186/s11671-019-3111-y>.
- [54] N. Ollier, Y. Fuchs, O. Cavani, A.H. Horn, S. Rossano, Influence of impurities on Cr³⁺ luminescence properties in Brazilian emerald and alexandrite, *Eur. J. Mineral* 27 (2015) 783–792, <https://doi.org/10.1127/ejm/2015/0027-2484>.
- [55] V.S. Gorelik, A.E. Kozhevnikov, S.N. Mikov, P.P. Sverbil, M.M. Stepanov, Laser spectroscopy of nanocrystals of aluminum and silicon oxides, *J. Russ. Laser Res.* 28 (2007) 55–102, <https://doi.org/10.1007/s10946-007-0004-9>.
- [56] M. Popov, V. Churkin, A. Kirichenko, V. Denisov, D. Ovsyannikov, B. Kulnitskiy, I. Perezhogin, V. Aksenonkov, V. Blank, Raman spectra and bulk modulus of nanodiamond in a size interval of 2–5 nm, *Nanoscale Res. Lett.* 12 (2017) 561, <https://doi.org/10.1186/s11671-017-2333-0>.
- [57] V.I. Korepanov, H. Hamaguchi, E. Osawa, V. Ermolenkov, I.K. Lednev, B.J. M. Etzold, O. Levinson, B. Zousman, C.P. Epperla, H.-C. Chang, Carbon structure in nanodiamonds elucidated from Raman spectroscopy, *Carbon* 121 (2017) 322–329, <https://doi.org/10.1016/j.carbon.2017.06.012>.
- [58] M. Mermoux, S. Chang, H.A. Girard, J.-C. Arnault, Raman spectroscopy study of detonation nanodiamond, *Diam. Relat. Mater.* 87 (2018) 248–260, <https://doi.org/10.1016/j.diamond.2018.06.001>.
- [59] Y. Inamura, Y. Katayama, W. Utsumi, K. Funakoshi, Transformations in the intermediate-range structure of SiO₂ glass under high pressure and temperature, *Phys. Rev. Lett.* 93 (2004) 015501, <https://doi.org/10.1103/PhysRevLett.93.015501>.
- [60] A. Arasuna, M. Okuno, T. Mizukami, M. Akaogi, T. Yokoyama, H. Okudera, S. Arai, The role of water in coesite crystallization from silica gel, *Eur. J. Mineral* 25 (2014) 791–796, <https://doi.org/10.1127/0935-1221/2013/0025-2331>.
- [61] V.S. Efimchenko, V.K. Fedotov, M.A. Kuzovnikov, A.S. Zhuravlev, B.M. Bulychev, Hydrogen solubility in amorphous silica at pressures up to 75 kbar, *J. Phys. Chem. B* 117 (2013) 422–425, <https://doi.org/10.1021/jp309991x>.
- [62] K.P. Meletov, V.S. Efimchenko, M.A. Korotkova, V.M. Masalov, N.S. Sukhinina, G. A. Emel'chenko, Peculiarities of the absorption and desorption of hydrogen by opal matrices, *Int. J. Hydrogen Energy* 48 (2023) 14337–14347, <https://doi.org/10.1016/j.ijhydene.2022.12.297>.
- [63] M. Popov, F. Khorobrykh, S. Klimin, V. Churkin, D. Ovsyannikov, A. Kvashnin, Surface tamm states of 2–5 nm nanodiamond via Raman spectroscopy, *Nanomaterials* 13 (2023) 696, <https://doi.org/10.3390/nano13040696>.
- [64] A.S. Naumova, S.V. Lepeshkin, A.R. Oganov, Hydrocarbons under pressure: phase diagrams and surprising new compounds in the C–H system, *J. Phys. Chem. C* 123 (2019) 20497–20501, <https://doi.org/10.1021/acs.jpcc.9b01353>.
- [65] G. Liu, Z. Zhao, M. Sun, J. Li, G. Hu, X. Wang, New insights into natural gas diffusion coefficient in rocks, *Petrol. Explor. Dev.* 39 (2012) 597–604, [https://doi.org/10.1016/S1876-3804\(12\)60081-0](https://doi.org/10.1016/S1876-3804(12)60081-0).